Buck Converter Modeling in High Frequency using Several Transfer Function-based Approaches

Imen Shiri, Sanda Lefteriu and Cécile Labarre
Unité de Recherche en Informatique et Automatique, IMT Lille Douai, 941, rue Charles Bourseul, 59500 Douai, France

Keywords: Buck Converter, Modeling, Transfer Function, High Frequency, Parasitic Elements.

Abstract: The recent development of large gap (GaN) components adapted to high frequency operation opens up interesting perspectives for the emergence of high power density static converters. However, the implementation of GaN components requires the development of new characterization, modeling and design methods adapted to these fast components. In this paper, we present three modeling techniques for a static converter in the frequency domain. They are all characterizing the input - output transfer function and they are: the average model, the generalized transfer function (GTF) and the modified nodal analysis technique (MNA). These models, already existing in the literature, are extended to account for the parasitic effects of the switching elements (diodes or transistors). In fact, parasitic elements associated with the different passive and active components are inherent in a power electronics structure. Their effects are negligible in low frequency but they are preponderant in high frequency. Simulation results performed for a Buck converter show that, while the GTF and the MNA are able to predict the resonances present at multiples of the switching frequency, the average model does not. In terms of the influence of the parasitic elements on the transfer function, the peak which is due to the output filter parameters is attenuated. Lastly, the experimental validation shows that, even with the introduction of the parasitic elements of the switching components, there are still discrepancies between the models and the data, so additional parasitics still need to be accounted for.

1 INTRODUCTION

Static converters allow the electric power source (a battery, the electrical network, a solar panel, etc.) to be adapted to the needs of the receiver (an electric motor, an asynchronous machine, etc.). In the literature, time domain models, based on the analysis of the converter's dynamics described by differential equations, have been proposed : state space averaging (SSA) (Biolkova et al., 2010) (Behjati et al., 2013) (Anun et al., 2013), the hybrid model (Benmansour, 2009) to name a few. Frequency domain models have also been proposed, such as the average model, the GTF (Biolek et al., 2006) and the MNA (Trinchero, 2015). With the improvement of switching component's performance (IGBT, diode) such as the speed, these models describing the frequency behavior should be developped further. Our objective is to describe the behavior of a converter in the frequency domain using the transfer function.

Power converters contain diodes and transistors, hence they fall under the category of switching systems. These switches move between an ON state and an OFF state periodically. Thus, neglecting non-idealities, power converters can be considered as linear periodic systems varying in time. For this reason, the concept of the transfer function needs to be redefined and adapted.

To start with, we are interested in the Buck DC-DC converter, which can be used for the control of DC motors, to regulate the speed of rotation of a DC motor in both directions of rotation, battery chargers, solar chargers, etc.

The average model describes the dynamics of the system as a function of the average values for the current and voltage variables, thus neglecting the effects due to switching. The Generalized Transfer Function (Biolek, 1997) is based on the small signal analysis technique to obtain the transfer function. It combines the continuous behavior (due to storage elements) and discrete behavior (due to switches) with a single transfer function. Since DC-DC converters are considered as periodic switched linear systems (PSL), they can be characterized by a time-variant transfer function, which takes into account

Shiri, I., Lefteriu, S. and Labarre, C.
Buck Converter Modeling in High Frequency using Several Transfer Function-based Approaches.
DOI: 10.5220/0007927407220729
In *Proceedings of the 16th International Conference on Informatics in Control, Automation and Robotics (ICINCO 2019)*, pages 722-729
ISBN: 978-989-758-380-3

the time-varying behavior, or alternatively, by the bi-frequency transfer function. For such circuits, their steady-state response may be found as the solution of a MNA equation (Trinchero, 2015).

This paper is a follow-up to the publication (Lefteriu and Labarre, 2016). It compares the three transfer function modeling techniques for computing the magnitude of the frequency response of a Buck converter, this time integrating the parasitic elements of the diode and the transistor. Ideally, switching should be between 0 and the final value instantaneously. To obtain an improved frequency model, wide-bandwidth components have to be considered: equivalent series resistance, lumped shunt parasitic capacitance (Davoudi, 2010). Adding these components complicates models already proposed. As a first contribution of our paper, the average model was rederived using the descriptor system (Verghese et al., 1981). As a second contribution, the GTF (Biolek et al., 2006) and the MNA (Trinchero, 2015) were adapted to the new setting.

This paper is structured as follows. In Sect. 2, we describe the effects of parasitics on the switching signals. In Sect. 3, the Buck converter with parasitic elements is described in terms of the average model. In Sect. 4, the modeling technique using the generalized transfer function is re-derived. The extension of the technique proposed in (Trinchero, 2015) is presented in Sect. 5. Sect. 6 presents simulation results and, finally, the conclusion and directions for future research are given in Sect. 7.

2 EFFECTS OF PARASITIC ELEMENTS ON THE SWITCHING SIGNALS

The Buck converter is a hybrid dynamical system with the continuous behavior dictated by the linear time-invariant elements (resistor, capacitor, inductor) and the discrete behavior given by the switches (transistor, diode). Fig. 1 shows the topology of a Buck converter which supplies a passive load resistor with the voltage V_{out}.

The IGBT is represented by the switch S and the diode by the switche $\overline{S}$. The switch S is controlled by a pulse width modulation signal (PWM), a binary input signal. When $S = 1$, the switch is closed (conducting), and for $S = 0$ the switch is open (non-conducting).

Fig. 2 shows the case of ideal switching and the voltage measured across the IGBT. The plot for V_{ds} in Fig. 2b shows an exponentially decaying sinusoidal

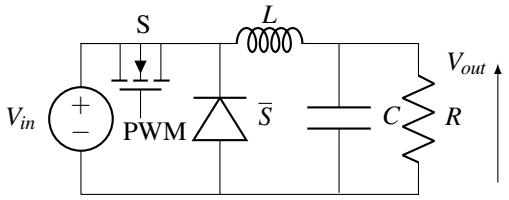

Figure 1: Topology of the Buck converter.

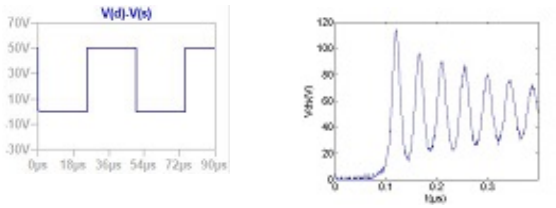

(a) Ideal swiching (b) IGBT switching

Figure 2: Voltage in case of ideal switching and across the IGBT.

signal which can be explained by the presence of a second-order circuit given by parasitic RLC elements.

As in any semiconductor component, there is a parasitic capacitance in the IGBT and diode that models the inverse polarized P-N junction and disrupts the operation in high frequency. This capacitance will be set in parallel. To obtain the ripples, the IGBT and the diode will be modeled, in addition to the ideal switches, by an equivalent series resistance, and an equivalent series inductance. Fig. 3 shows the proposed model taking into account parasitics for an IGBT and a diode.

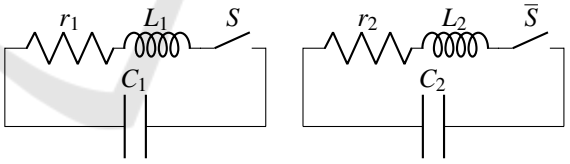

(a) IGBT (b) Diode

Figure 3: Equivalent models.

Integrating the proposed models into the Buck converter, Fig. 4 shows the topology of the Buck converter from Fig. 1 with parasitic elements. We have also accounted for the line inductance L_s.

3 AVERAGE MODEL

In continuous current mode (CCM), the current in the inductor never reachs zero and the Buck converter is described by two circuit typologies, namely:

- $S = 1, \overline{S} = 0$ in the time interval $t \in [kT, (k+\alpha)T]$

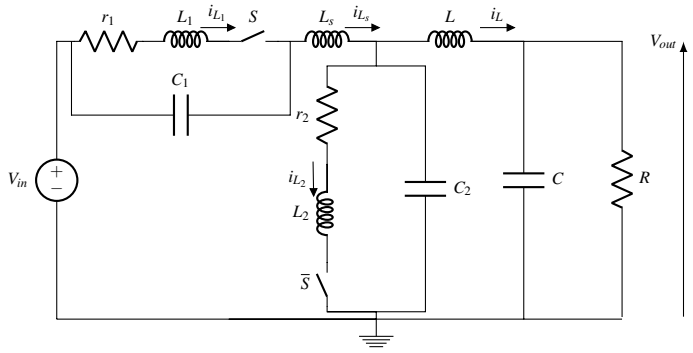

Figure 4: Topology of the Buck converter with parasitic elements.

- $S = 0, \overline{S} = 1$ for $t \in [(k+\alpha)T, (k+1)T]$,

with T, the switching period and $k = 0, 1, 2, \ldots$. The duty cycle α indicates the percentage of time that the switch S is ON during the switching period. In each of these operation modes, the behavior is linear, hence the circuit can be modeled by differential equations involving the inductors' currents i_{Ls} i_{L1}, i_{L2}, i_L and the voltages over the capacitors V_{c1},V_{c2}, V_c. The introduction of parasitic inductances in series with the switches results in the current variables through the switches being 0 during one of the two operating modes. Eventually, this yields to state equations with different state variables depending on the mode, hence a descriptor-form representation of the circuit is more appropriate. A descriptor system is of the form (Verghese et al., 1981):

$$\begin{aligned} \mathbf{E}\dot{\mathbf{x}}(t) &= \mathbf{A}\mathbf{x}(t) + \mathbf{B}V_{in}(t) \\ V_{out}(t) &= \mathbf{C}\mathbf{x}(t) + \mathbf{D}V_{in}(t), \end{aligned} \tag{1}$$

with the matrix $\mathbf{E}$ non-invertible. In our case, the state vector contains the variables i_{Ls} i_{L1}, i_{L2}, i_L, V_{c1},V_{c2}, V_c, hence it has dimension 7. This yields $\mathbf{E}$ and $\mathbf{A}$ of dimension 7×7, while $\mathbf{B}$ and $\mathbf{C}^T$ are of dimension 7×1. Lastly, $\mathbf{D}$ is scalar.

In the first mode, $i_{L2} = 0$, hence

$$\mathbf{E}_{1\,i,j} = \begin{cases} 0, & i \neq j \ \ \& \ \ i = j = 3 \\ 1, & i = j \neq 3 \end{cases} \tag{2}$$

$$\mathbf{A}_1 = \begin{pmatrix} 0 & 0 & 0 & 0 & -\frac{1}{L_s} & -\frac{1}{L_s} & 0 \\ 0 & -\frac{r_1}{L_1} & 0 & 0 & \frac{1}{L_1} & 0 & 0 \\ 0 & 0 & 1 & 0 & 0 & 0 & 0 \\ 0 & 0 & 0 & 0 & 0 & \frac{1}{L} & -\frac{1}{L} \\ \frac{1}{C_1} & -\frac{1}{C_1} & 0 & 0 & 0 & 0 & 0 \\ \frac{1}{C_2} & 0 & 0 & -\frac{1}{C_2} & 0 & 0 & 0 \\ 0 & 0 & 0 & \frac{1}{C} & 0 & 0 & -\frac{1}{RC} \end{pmatrix} \tag{3}$$

$$\mathbf{B} = \begin{pmatrix} \frac{1}{L_s} & 0 & 0 & 0 & 0 & 0 & 0 \end{pmatrix}^T \tag{4}$$

$$\mathbf{C} = \begin{pmatrix} 0 & 0 & 0 & 0 & 0 & 0 & 1 \end{pmatrix} \tag{5}$$

$$\mathbf{D} = 0. \tag{6}$$

Similarly, in the second mode, $i_{L1} = 0$, hence

$$\mathbf{E}_{2\,i,j} = \begin{cases} 0, & i \neq j \ \ \& \ \ i = j = 2 \\ 1, & i = j \neq 2 \end{cases} \tag{7}$$

$$\mathbf{A}_2 = \begin{pmatrix} 0 & 0 & 0 & 0 & -\frac{1}{L_s} & -\frac{1}{L_s} & 0 \\ 0 & 1 & 0 & 0 & 0 & 0 & 0 \\ 0 & 0 & -\frac{r_2}{L_2} & 0 & 0 & \frac{1}{L_2} & 0 \\ 0 & 0 & 0 & 0 & 0 & \frac{1}{L} & -\frac{1}{L} \\ \frac{1}{C_1} & 0 & 0 & 0 & 0 & 0 & 0 \\ \frac{1}{C_2} & 0 & -\frac{1}{C_2} & -\frac{1}{C_2} & 0 & 0 & 0 \\ 0 & 0 & 0 & \frac{1}{C} & 0 & 0 & -\frac{1}{RC} \end{pmatrix} \tag{8}$$

and $\mathbf{B}$, $\mathbf{C}$, $\mathbf{D}$ are the same as in Eq. (4)-(6).

The average model neglects the switching effects and considers the average value of the state variables over the switching period. This amounts to considering the average of the descriptor matrices in the two operating modes:

$$\mathbf{E} = \alpha\mathbf{E}_1 + (1-\alpha)\mathbf{E}_2 \tag{9}$$

$$\mathbf{A} = \alpha\mathbf{A}_1 + (1-\alpha)\mathbf{A}_2. \tag{10}$$

The average of the $\mathbf{B}$, $\mathbf{C}$, $\mathbf{D}$ in the two modes yields the same expressions as in Eq. (4)-(6). This results in an equation of the form (1) and the transfer function can be easily obtained by applying the Laplace transform:

$$H_{avg}(s) = \frac{V_{out}(s)}{V_{in}(s)} = \mathbf{C}(s\mathbf{E} - \mathbf{A})^{-1}\mathbf{B} + \mathbf{D}. \tag{11}$$

4 GENERALIZED TRANSFER FUNCTION (GTF)

The development of the Generalized Transfer Function relies on the solution to the state-space differential equation

$$\dot{\mathbf{x}}(t) = \mathbf{A}\mathbf{x}(t) + \mathbf{B}V_{in}(t). \tag{12}$$

The solution for the state $\mathbf{x}(t)$ depends on the initial condition $\mathbf{x}_0$ at time t_0 and the input $V_{in}(t)$ (Antoulas,

2005):

$$\mathbf{x}(t) = e^{\mathbf{A}(t-t_0)}\mathbf{x}(t_0) + \int_{t_0}^{t} e^{\mathbf{A}\tau}\mathbf{B}V_{in}(t-\tau)d\tau, \;\; t \geq t_0. \tag{13}$$

The reason why a standard-state space formulation is considered here, instead of the descriptor-form, is because the solution equivalent to (13) would be more difficult to derive. However, the descriptor realization with the singular $\mathbf{E}$ is not needed, as long as special care is taken to account for the zero state variables present in each mode.

In mode 1, the state variable $i_{L2} = 0$, hence the circuit can be modeled by differential equations of the form (12) involving the remaining non-zero state-variables. The resulting state-space matrix $\mathbf{A}_1$ is obtained by deleting the 3^{rd} row and column of the matrix in (3). Naturally, the $\mathbf{B}$ and $\mathbf{C}$ are the same as in (4)-(5), but without the 3^{rd} entry. Evaluating the solution (13) at the end of phase 1 ($t \in [kT, kT+\alpha T]$), we obtain:

$$\mathbf{x}_1(kT+\alpha T) = e^{\mathbf{A}_1\alpha T}\mathbf{x}_1(kT) + \int_{kT}^{kT+\alpha T} e^{\mathbf{A}_1\tau}\mathbf{B}_1 V_{in}(kT+\alpha T-\tau)d\tau. \tag{14}$$

Accounting for $i_{L2} = 0$, we obtain the state vector $\mathbf{x}(t)$ by premultiplying $\mathbf{x}_1(t)$ with the matrix $\mathbf{P}_1 \in \mathbf{R}^{7\times 6}$:

$$\mathbf{x}(t) = \mathbf{P}_1\mathbf{x}_1(t), \text{ where } \mathbf{P}_1 = \begin{pmatrix} 1 & 0 & 0 & 0 & 0 & 0 \\ 0 & 1 & 0 & 0 & 0 & 0 \\ 0 & 0 & 0 & 0 & 0 & 0 \\ 0 & 0 & 1 & 0 & 0 & 0 \\ 0 & 0 & 0 & 1 & 0 & 0 \\ 0 & 0 & 0 & 0 & 1 & 0 \\ 0 & 0 & 0 & 0 & 0 & 1 \end{pmatrix}.$$

In mode 2, the state variable $i_{L1} = 0$ and the circuit can be modeled by differential equations of the form (12) involving the remaining non-zero state-variables. The resulting state-space matrix $\mathbf{A}_2$ is obtained by deleting the 2^{nd} row and column of the matrix in (8). Naturally, $\mathbf{B}$ and $\mathbf{C}$ are the same as in (4)-(5), but without the 2^{nd} entry. Evaluating the solution (13) at the end of phase 2 ($t \in [kT+\alpha T, kT+T]$), we obtain:

$$\mathbf{x}_2(kT+T) = e^{\mathbf{A}_2(1-\alpha)T}\mathbf{x}_2(kT+\alpha T) + \int_{kT+\alpha T}^{kT+T} e^{\mathbf{A}_2\tau}\mathbf{B}_2 V_{in}(kT+T-\tau)d\tau. \tag{15}$$

Accounting for $i_{L1} = 0$, we obtain the state vector $\mathbf{x}(t)$ by premultiplying $\mathbf{x}_2(t)$ with the matrix $\mathbf{P}_2 \in \mathbf{R}^{7\times 6}$:

$$\mathbf{x}(t) = \mathbf{P}_2\mathbf{x}_2(t), \text{ where } \mathbf{P}_2 = \begin{pmatrix} 1 & 0 & 0 & 0 & 0 & 0 \\ 0 & 0 & 0 & 0 & 0 & 0 \\ 0 & 1 & 0 & 0 & 0 & 0 \\ 0 & 0 & 1 & 0 & 0 & 0 \\ 0 & 0 & 0 & 1 & 0 & 0 \\ 0 & 0 & 0 & 0 & 1 & 0 \\ 0 & 0 & 0 & 0 & 0 & 1 \end{pmatrix}.$$

We replace (14) into (15):

$$\mathbf{x}(kT+T) = e_0^{\mathbf{A}_2(1-\alpha)T} e_0^{\mathbf{A}_1\alpha T}\mathbf{x}(kT) + e_0^{\mathbf{A}_2(1-\alpha)T}\int_{kT}^{kT+\alpha T} e_0^{\mathbf{A}_1\tau}\mathbf{P}_1\mathbf{B}_1 V_{in}(kT+\alpha T-\tau)d\tau + \int_{kT+\alpha T}^{kT+T} e_0^{\mathbf{A}_2\tau}\mathbf{P}_2\mathbf{B}_2 V_{in}(kT+T-\tau)d\tau, \tag{16}$$

where $e_0^{\mathbf{A}_2}$ is a notation for $\mathbf{P}_2 e^{\mathbf{A}_2}\mathbf{P}_2^T$ and $e_0^{\mathbf{A}_1}$ is a notation for $\mathbf{P}_1 e^{\mathbf{A}_1}\mathbf{P}_1^T$. Naturally, $\mathbf{P}_1^T\mathbf{P}_1 = \mathbf{I}$ and $\mathbf{P}_2^T\mathbf{P}_2 = \mathbf{I}$, where $\mathbf{I}$ is the identity matrix. Hence, $\mathbf{P}_1^T\mathbf{B}_1 = \mathbf{P}_2^T\mathbf{B}_2 = \mathbf{B}$, with $\mathbf{B}$ given in (4).

Applying the small signal analysis, the input is taken as a constant voltage together with a small amplitude AC component $V_{in}(t) = V_0 + \tilde{V}_{in}e^{j\Omega t}$, $V_0 >> \tilde{V}_{in}$ with Ω, the perturbation frequency of choice. The steady-state output voltage will be composed of a DC component and several AC components. By analogy with linear-time invariant systems, only the component with frequency Ω is of interest, the other frequencies which appear due to the non-linearity of the overall system being disregarded. The generalized transfer function for the line-to-output response is given by evaluating $H_{GTF}(s)$ on the imaginary axis at $s = j\Omega$ for various values of Ω:

$$H_{GTF}(s) = \mathbf{C}\left(\mathbf{I} - \mathbf{G}_2\mathbf{G}_1 z^{-1}\right)^{-1}\left(\mathbf{G}_2\hat{\mathbf{H}}_1(s)z^{-(1-\alpha)} + \hat{\mathbf{H}}_2(s)\right)$$

where $z = e^{sT}$ and

$$\mathbf{G}_1 = e_0^{\mathbf{A}_1\alpha T}$$
$$\mathbf{G}_2 = e_0^{\mathbf{A}_2(1-\alpha)T}$$
$$\mathbf{H}_1(s) = \int_0^{\alpha T} e_0^{\mathbf{A}_1\tau}\mathbf{B}e^{-s\tau}d\tau$$
$$\mathbf{H}_2(s) = \int_{\alpha T}^{T} e_0^{\mathbf{A}_2\tau}\mathbf{B}e^{-s\tau}d\tau.$$

5 AUGMENTED MNA FOR PSL CIRCUITS

This section applies the approach initially proposed in (Trinchero, 2015) for the computation of the steady-state of periodic switched linear circuits, to the computation of the small-signal transfer function

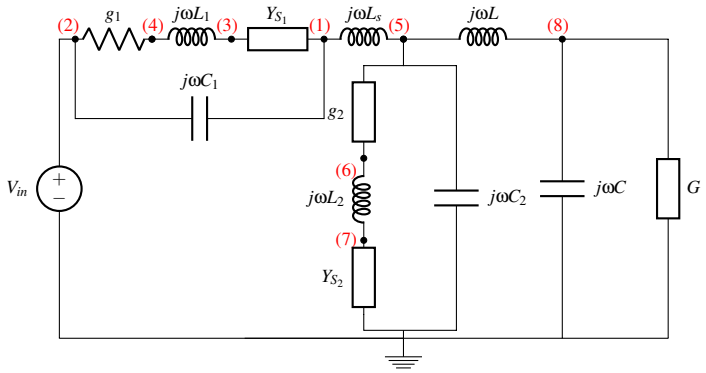

Figure 5: Frequency domain representation of the Buck converter with parasitic elements.

of Buck converters which accounts for parasitic elements. The bi-frequency transfer function is:

$$H(\omega,\Omega)=\int_{-\infty}^{\infty}\int_{-\infty}^{\infty}h(t,\tau)e^{-j(\omega t-\Omega\tau)}dtd\tau \quad (17)$$

and the output in the frequency domain is :

$$Y(\omega)=\frac{1}{2\pi}\int_{-\infty}^{\infty}H(\omega,\Omega)U(\Omega)d\Omega, \quad (18)$$

where U is the input, Ω and ω are the input and output frequencies. This shows that a sinusoidal input with frequency Ω produces an output with a rich spectrum, as opposed to LTI systems, for which the output contains solely the frequency Ω. The time-varying transfer function $H(t,\Omega)=\int_{-\infty}^{\infty}h(t,\tau)e^{-j\Omega(t-\tau)}d\tau$, is related to the bi-frequency transfer function as

$$H(\omega,\Omega)=\int_{-\infty}^{\infty}H(t,\Omega)e^{j(\Omega-\omega)t}dt. \quad (19)$$

For periodically switched linear circuits, $H(t,\Omega)$ is a periodic function of t which can be written as a Fourier series with respect to the switching frequency $\omega_s=\frac{2\pi}{T}$:

$$H(t,\Omega)=\sum_{n=-\infty}^{n=\infty}H_n(\Omega)e^{jn\omega_s t}, \quad (20)$$

with the frequency-dependent Fourier coefficients $H_n(\Omega)$ called aliasing transfer functions:

$$H_n(\Omega)=\frac{1}{T}\int_0^T H(t,\Omega)e^{-jn\omega_s t}dt.$$

The output in the frequency domain is obtained by substituting (19) and (20) into (18):

$$Y(\omega)=\sum_{n=-\infty}^{n=\infty}H_n(\omega-n\omega_s)U(\omega-n\omega_s). \quad (21)$$

The frequency domain representation of a Buck converter is obtained by substituting the switch S and $\overline{S}$ in Fig. 4 with the periodic switching admittance element respectively Y_{S1} and Y_{S2}. Fig. 5 shows the frequency domain representation of the buck converter with parasitcis elements. Compared to the model proposed by (Trinchero, 2015), the MNA equation will be modified to account for the presence of L_i, r_i, C_i , i=1,2, yielding:

$$\left[\begin{array}{c|c}\mathbf{M}(\omega) & \mathbf{H}\\ \hline \mathbf{H}^T & \mathbf{N}(\omega)\end{array}\right]\left[\begin{array}{c}\mathbf{V}(\omega)\\ \hline \mathbf{I}(\omega)\end{array}\right]=\left[\begin{array}{c}\mathbf{G}(\omega)\\ \hline \mathbf{F}(\omega)\end{array}\right], \quad (22)$$

where:

$$\mathbf{V}(\omega)=(V_1 \quad V_2 \quad V_3 \quad V_4 \quad V_5 \quad V_6 \quad V_7 \quad V_8)^T \quad (23)$$

$$\mathbf{I}(\omega)=(I_{L_s} \quad I_{L_1} \quad I_{L_2} \quad I_L)^T \quad (24)$$

$$\mathbf{G}(\omega)=(0 \quad 0 \quad 0 \quad 0 \quad 0 \quad 0 \quad 0 \quad 0)^T \quad (25)$$

$$\mathbf{F}(\omega)=(-V_{in} \quad 0 \quad 0 \quad 0)^T \quad (26)$$

$$\mathbf{H}^T=\begin{pmatrix}\mathbf{I} & -\mathbf{I} & 0 & 0 & -\mathbf{I} & 0 & 0 & 0\\ 0 & 0 & -\mathbf{I} & \mathbf{I} & 0 & 0 & 0 & 0\\ 0 & 0 & 0 & 0 & 0 & \mathbf{I} & -\mathbf{I} & 0\\ 0 & 0 & 0 & 0 & \mathbf{I} & 0 & 0 & -\mathbf{I}\end{pmatrix} \quad (27)$$

$$\mathbf{N}(\omega)=\begin{pmatrix}-j\boldsymbol{\omega}L_S & 0 & 0 & 0\\ 0 & -j\boldsymbol{\omega}L_1 & 0 & 0\\ 0 & 0 & -j\boldsymbol{\omega}L_2 & 0\\ 0 & 0 & 0 & -j\boldsymbol{\omega}L\end{pmatrix} \quad (28)$$

$$\mathbf{M}(\omega)=\begin{pmatrix}a & -h & -c_1 & 0 & 0 & 0 & 0 & 0\\ -h & b_1 & 0 & -d_1 & 0 & 0 & 0 & 0\\ -c_1 & 0 & c_1 & 0 & 0 & 0 & 0 & 0\\ 0 & -d_1 & 0 & d_1 & 0 & 0 & 0 & 0\\ 0 & 0 & 0 & 0 & b_2 & -d_2 & 0 & 0\\ 0 & 0 & 0 & 0 & -d_2 & d_2 & 0 & 0\\ 0 & 0 & 0 & 0 & 0 & 0 & c_2 & 0\\ 0 & 0 & 0 & 0 & 0 & 0 & 0 & f\end{pmatrix} \quad (29)$$

where $a=j\boldsymbol{\omega}C_1+\mathbf{Y}_{s_1}$,
$h=j\boldsymbol{\omega}C_1$,

$b_i = j\boldsymbol{\omega}C_i + g_i$, where $g_i = \frac{1}{r_i}$, $i = 1,2$,
$c_i = \mathbf{Y}_{s_i}$, $i = 1,2$,
$d_i = g_i\mathbf{I}$, $i = 1,2$,
$f = j\boldsymbol{\omega}C + G$, where $G = \frac{1}{R}$.

Each block in (22) is of dimension $2N+1$. Ideally, N should be large because we are computing an infinite sum as shown in (21). In particular, the matrix $\boldsymbol{\omega}$ is equal to

$$\boldsymbol{\omega} = diag\big(\big[\omega_0 - N\omega_s \ldots \omega_0 - \omega_s \ \omega_0 \ \omega_0 + \omega_s \ldots \omega_0 + N\omega_s\big)\big]$$

where ω_0 is the excitation frequency. Moreover, $\mathbf{Y}_{s_1}$ and $\mathbf{Y}_{s_2}$ are matrices of the form

$$\mathbf{Y}_{s_i} = \begin{bmatrix} Y_{i,0} & Y_{i,-1} & \ldots & Y_{i,-2N} \\ Y_{i,1} & Y_{i,0} & \ldots & Y_{i,-2N+1} \\ \vdots & \vdots & \ddots & \vdots \\ Y_{i,2N} & Y_{i,2N-1} & \ldots & Y_{i,0} \end{bmatrix}, \ i = 1,2 \tag{30}$$

where $Y_{1,n}$ are the Fourier coefficients of the window function with amplitude 1 and period T_s when the switch S is on:

$$Y_{1,n} = f_s \int_0^{\alpha T} e^{-jn\omega_s t} dt = \frac{e^{-jn\omega_s \alpha T} - 1}{-j2\pi n}, \ n = -2N, \ldots, 2N,$$

and $Y_{2,n}$ are the Fourier coefficients of the same window function delayed by αT for $\bar{S}$: $Y_{2,n} = Y_{1n} e^{-j\omega_s n\alpha T}$, $n = -2N, \ldots, 2N$.

Last, but not least, the unknowns in (23)-(24) contain the coefficients of the truncated frequency domain representation with $2N+1$ terms. For example, for I_L, this would be $I_L(\omega) = \sum_{n=-N}^{N} I_n \delta(\omega - n\omega_s - \omega_0)$.

Small-signal analysis assumes an input obtained from the superposition of a constant and a small-amplitude AC component $V_{in}(t) = V_0 + \tilde{V}_{in} e^{j\Omega t}$, with $V_0 >> \tilde{V}_{in}$ and Ω, the perturbation frequency of choice. This corresponds to a sum of 2 Dirac distributions in the frequency domain:

$$V_{in}(\omega) = V_0 \delta(\omega) + \tilde{V}_{in} \delta(\omega - \Omega).$$

Hence, the linear system in (22) should be solved for each value of the excitation frequency $\omega_0 = 0$ and $\omega_0 = \Omega$. The output voltage is the voltage at node 8 in Fig. 5 and is expressed as $V_8 = V_{8,DC} + V_{8,AC}$, where

$$V_{8,DC}(\omega) = \sum_{n=-N}^{N} V_{n,DC} \delta(\omega - n\omega_s), \tag{31}$$

$$V_{8,AC}(\omega) = \sum_{n=-N}^{N} V_{n,AC} \delta(\omega - n\omega_s - \Omega), \tag{32}$$

with the coefficients $V_{n,DC}$ and $V_{n,AC}$ found by solving the linear system in (22) for $\omega_0 = 0$ and $\omega_0 = \Omega$, respectively. The transfer function at perturbation frequency Ω is

$$H_{MNA}(j\Omega) = \begin{cases} \frac{V_{0,AC}}{\tilde{u}}, & \text{if } \Omega \neq n\omega_s \\ \frac{V_{n,DC} + V_{0,AC}}{\tilde{u}}, & \text{if } \Omega = n\omega_s \end{cases}. \tag{33}$$

When the perturbation frequency Ω is an integer multiple of the switching frequency ω_s, there are components due to the DC input which also contribute to the response.

6 RESULTS

Simulation results comparing the three modeling techniques detailed in the previous sections, namely the average model, the Generalized Transfer Function and the augmented MNA, are applied to a Buck converter with and without parasitics. The parameters for the Buck converter are $L = 1$mH, $C = 500\mu$F, $R = 12\Omega$. For simplicity, we considered that the IGBT and the diode have the same values for the parasitic elements: $L_1 = L_2 = 100$nH, $C_1 = C_2 = 1.4$nF and $r_1 = r_2 = 0.2\Omega$. The line inductance is taken as $L_s = 500$nH. The switching frequency is $f_s = 20$kHz$= \frac{1}{T}$ and the duty cycle is $\alpha = \frac{1}{2}$.

For comparison, the magnitude of the Bode plot was measured with an Agilent spectrum analyzer operating between 9kHz and 3GHz. For low frequencies, measurements were performed with an oscilloscope.

Fig. 6 shows the frequency response obtained with the average model in the ideal case and when including parasitics. The two average models do not predict the peaks due to switching. The amplitude of the low frequency resonance (due to the converter output filter) is slightly smaller when including parasitic elements. Moreover, the average model with parasitics detects a high frequency resonance at around $f = 15$MHz. These observations are explained by the poles of the two models shown in Table 1. The ideal case corresponds to a second-order system with only two poles, while the parasitics add 5 more poles.

Table 1: Poles of the two average models: with and without parasitic elements.

With	without
$-1.8 \cdot 10^2 \pm 1.4 \cdot 10^3$i	$-8.3 \cdot 10^1 \pm 1.4 \cdot 10^3$i
$-6.1 \cdot 10^5$	0
$-5 \cdot 10^5 \pm 4.2 \cdot 10^7$i	0
$-1.9 \cdot 10^5 \pm 6.8 \cdot 10^7$i	0

From these values, we notice that the peak in low frequency is explained by the fact that the imaginary

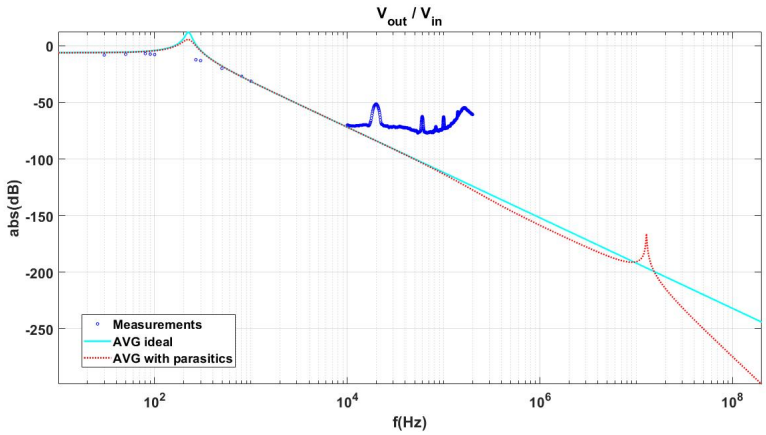

Figure 6: Simulation result: Average model.

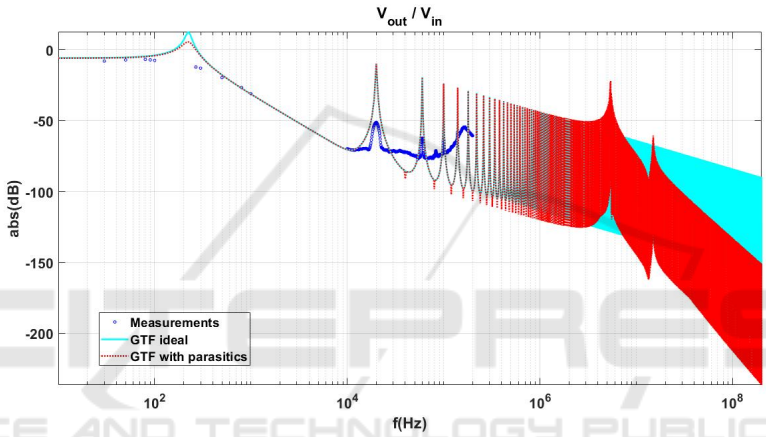

Figure 7: Simulation result: GTF.

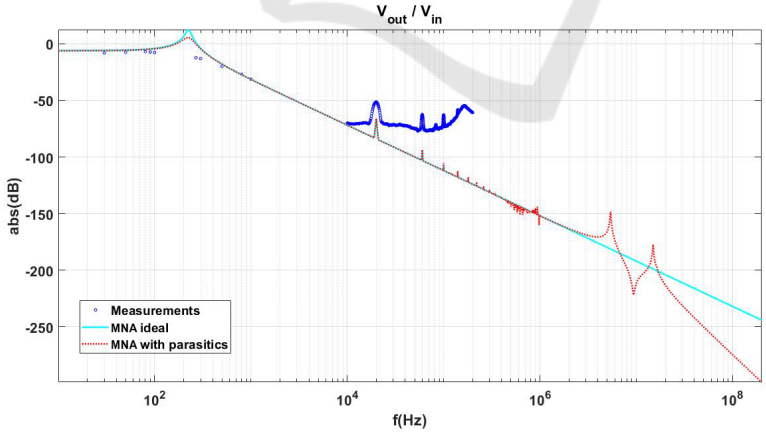

Figure 8: Simulation result: MNA.

part is almost identical and the real part decreases. In addition to that, two other pairs of complex conjugate poles appear at around $f = 15$MHz.

Fig. 7 shows the response computed with the generalized transfer function for the ideal case, as well as the case with parasitics. This approach predicts the peaks at odd multiples of the switching frequency (due to choosing the duty cycle as $\alpha = \frac{1}{2}$, the even multiples are not present). The amplitude of these peaks computed with GTF is higher than

those measured. In addition to these peaks, the GTF predicts two resonances at around 5.42MHz and 15 MHz for the case with parasitics.

Last, but not least, the response computed with the MNA approach is shown in Fig. 8. The MNA is also able to predict the peaks in the frequency response at odd multiples of the switching frequency, however, these peaks are decreasing in amplitude. The amplitude of these peaks is lower than those shown by the measurements. In addition to these peaks, the MNA predicts, as the GTF two resonances at around 5.43MHz and 14 MHz for the case with parasitics.

7 CONCLUSION AND FUTURE WORK

The transfer function for a Buck power converter with parasitic elements taken into consideration for the switching devices was computed with three approaches: the average model, the GTF and the MNA for PSL circuits. These approaches were compared against each other and against the measurements. Our analysis shows that the introduction of parasitic elements has an effect on the low frequency resonance, this resonance being due to the converter's output filter. Moreover, the GTF and MNA predict two additional peaks resonances at arround 5MHz and 14 MHz due to the parasitic's elements. At odd multiples of the switching frequency, we noticed a negligible effect of the parasitics. In the future, we will improve our model in the following ways. First, we will determine the correct values of the parasitic elements from the switching signal. Second, we will also take into consideration the parasitic elements of the output filter's inductance, capacitance and resistance.

ACKNOWLEDGEMENTS

This work has been achieved within the framework of the CE2I project (Convertisseur d'Energie Integre Intelligent). CE2I is co-financed by European Union with the financial support of European Regional Development Fund (ERDF), the French State and the French Region of Hauts-de-France.

REFERENCES

Antoulas, A. C. (2005). *Approximation of large-scale dynamical systems*, volume 6. SIAM.

Anun, M., Ordonez, M., and Luchino, F. (2013). Topology zero: A generalized averaging equivalent circuit model for basic DC-DC converters. In *2013 IEEE 14th Workshop on Control and Modeling for Power Electronics (COMPEL)*, pages 1–7.

Behjati, H., Niu, L., Davoudi, A., and Chapman, P. L. (2013). Alternative time-invariant multi-frequency modeling of PWM DC-DC converters. *IEEE Transactions on Circuits and Systems I: Regular Papers*, 60(11):3069–3079.

Benmansour, K. (2009). *Réalisation d'un banc d'essai pour la Commande et l'Observation des Convertisseurs Multicellulaires Série: Approche Hybride*. PhD thesis, Cergy-Pontoise.

Biolek, D. (1997). Modeling of periodically switched networks by mixed S-Z description. *IEEE Transactions on Circuits and Systems I: Fundamental Theory and Applications*, 44(8):750–758.

Biolek, D., Biolková, V., and Dobes, J. (2006). Modeling of switched DC-DC converters by mixed S-Z description. In *2006 IEEE International Symposium on Circuits and Systems*, pages 4–pp.

Biolkova, V., Kolka, Z., and Biolek, D. (2010). State-space averaging (SSA) revisited: on the accuracy of SSA-based line-to-output frequency responses of switched DC-DC converters. 2:1.

Davoudi, A. (2010). *Reduced-order modeling of power electronics components and systems*. PhD thesis, University of Illinois at Urbana-Champaign.

Lefteriu, S. and Labarre, C. (2016). Transfer function modeling for the buck converter. In *2016 IEEE 20th Workshop on Signal and Power Integrity (SPI)*, pages 1–4.

Trinchero, R. (2015). *EMI Analysis and Modeling of Switching Circuits*. PhD thesis, Politecnico di Torino.

Verghese, G., Lévy, B., and Kailath, T. (1981). A generalized state-space for singular systems. *IEEE Transactions on Automatic Control*, 26(4):811–831.